MPI 2015 - Flooding in Porous Media
W.L. Gore and Associates, Inc.

Daniel M. Anderson[1], Jordan Angel[2], Chris Breward[3], Pavel Dubovski[4], Dean Duffy[5], Ryan Evans[6], Zachary Grant[7], Amy Janett[6], Jiahua Jiang[7], Bethuel Khamala[8], Ruowen Liu[9], Zahra Niroobakhsh[10], Thierry Platini[11], Pejman Sanaei[12], Lan Zhong[6]

[1]George Mason University, Fairfax, VA 22030
[2]Rensselaer Polytechnic Institute, Troy, NY 12180
[3]University of Oxford, Oxford, OX2 6GG, UK
[4]Stevens Institute of Technology, Hoboken NJ 07030-5991
[5]NASA/Goddard Space Flight Center, Greenbelt, MD 20771
[6]University of Delaware, Newark, DE 19716
[7]University of Massachusetts Dartmouth, Dartmouth, MA 02747-2300
[8]The University of Texas at El Paso, El Paso, TX 79968
[9]Arizona State University, Tempe AZ 85281
[10]Penn State University, University Park, PA 16802
[11]Coventry University, Coventry, CV1 5FB, UK
[12]New Jersey Institute of Technology, University Heights Newark, NJ 07102

November 9, 2015

Abstract

The removal of pollutants such as sulfur dioxide (SO_2) from industrial exhaust before release into the atmosphere is of considerable environmental interest. One means of removing SO_2 is through a chemical reaction with water vapor in a porous filter composed of specially-designed solid particles or fibers. A product of this reaction is sulfuric acid which forms in the pore space of the filter. We discuss a mathematical description of this chemical reaction and develop models for transport of SO_2 in a porous filter and for the accompanying fluid production. Our goal is to improve the understanding of how transport and reaction processes occur and how the generation of fluid impacts the effectiveness of the filter. Flooding, which occurs when fluid in the pore space makes its way to the exterior of the filter, is of particular interest. Mathematical and computational models developed here may aid in understanding the underlying transport and reaction mechanisms and in improving filter efficiency.

Contents

1 Introduction

The design of effective filters plays a key role in a wide variety of environmental, medical, textile and other industrial settings. Filters are designed with a target application in mind and the mechanism(s) by which they function range from very simple to highly complex. An example of a filter that is based on a simple mechanical/geometrical concept is a fishing net – big fish get caught while small ones swim through the holes. In contrast, the filters of interest in the present context rely on complex interactions and transport of a multi-species gas through a reactive multiphase system whose geometry may be a complex network of fibers or a random packing of particles. Mass transport of multiple phases and multiple chemical species through such a network or porous media by diffusion and/or advection along with the accompanying chemical reactions must therefore be addressed in order to understand and optimize filter performance.

The particular situation of interest involves the removal of sulfur dioxide (SO_2) from an industrially-generated exhaust gas flowing into the outside environment through a channel (e.g. a 'smoke stack') through the placement of a filter (or filters) inside the channel. Consider a single filter whose exterior geometry is that of a 3D rectangular solid with one dimension much thinner than the others. Rather than placing such a filter across a channel in which the sulfur dioxide-carrying gas flows (a likely optimal fish-catching orientation of a net in a flowing river) the idea here is to place an array or stack of these thin filters (each separated by a certain distance from the one above or below it) so that the channel flow is along the large surface area of the filter (see Figure 1). The mechanism by which SO_2 is removed from the gas flowing through the channel involves (1) transport of SO_2 (e.g. by diffusion) into each filter orthogonal to the direction of the gas flow in the channel and (2) a chemical reaction of the SO_2 with the filter's carbon particles (or fibers) and water vapor to effectively remove SO_2 from the flow. As described in more detail below, a product of this reaction is a fluid – sulfuric acid – that occupies the pore space of the filter and has potential long term consequences of significantly reducing the effectiveness of the filter by blocking access of the reactant gas to catalyst sites on the solid particles and/or inhibiting or eliminating the transport of SO_2-carrying gas from the channel into the filter. The notion of 'flooding' characterizes the situation in which a sufficient amount of fluid is generated within the pore space of the filter and leads to the appearance of fluid build-up on the outside of the filter.

The goal of the present project is to develop a mathematical framework for characterizing fluid production and transport inside of a porous medium. Of particular interest is the prediction of time scales and spatial profiles associated with flooding of the filter pore space. We address three particular aspects of this problem. First, a description of the chemical reaction that involves the consumption of sulfur dioxide (SO_2) and the production of sulfuric acid (H_2SO_4) is given. Second, a network-based model for reactant transport and fluid generation within the pore space is derived and some preliminary calculations are presented. Third, a continuum model that characterizes the filter as a porous medium in which multispecies/multiphase transport occurs is developed and preliminary calculations are presented.

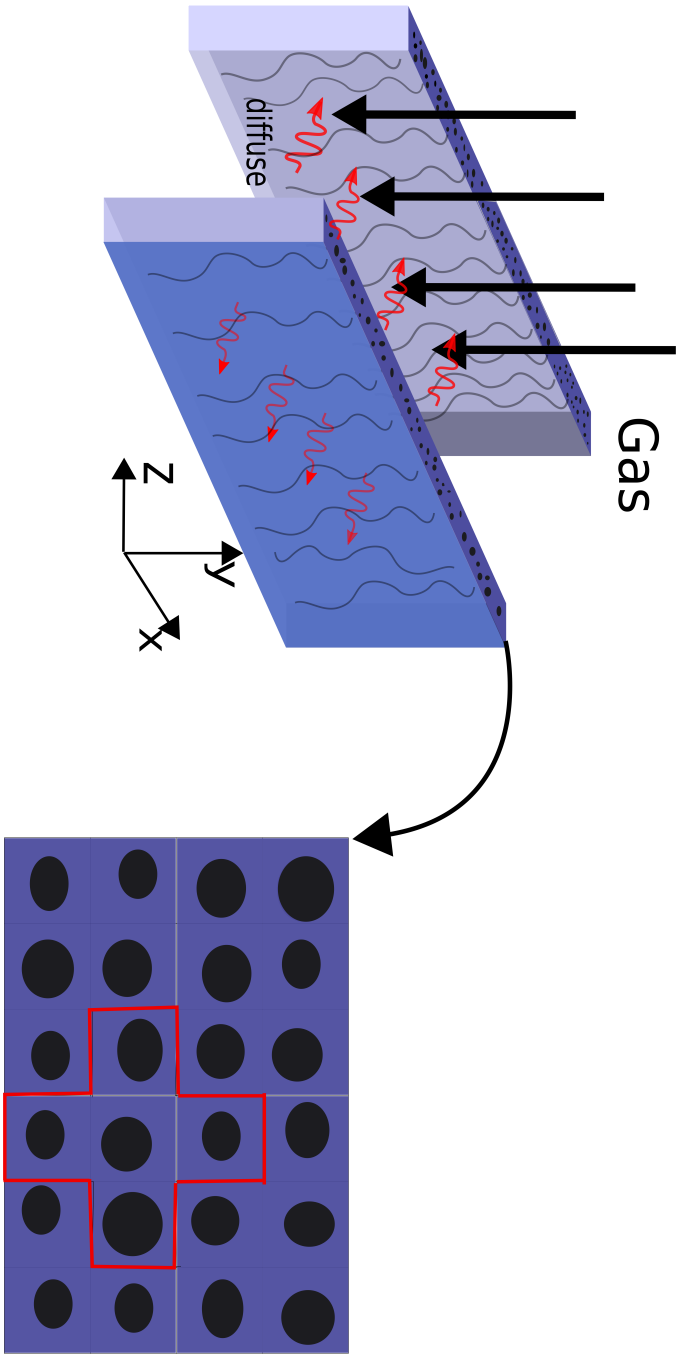

Figure 1: This figure shows a sketch of the basic filter/channel geometry.

2 Modeling the Chemical Reaction: Oxidation of Sulfur Dioxide

Our first step towards a working filtration model involves an understanding of the chemical reactions that may occur within the filter. The description used here is based

on the work of Govindarao and Gopalakrishna [5], who studied the oxidation of sulfur dioxide in an aqueous environment of carbon catalysts. In this section we outline details of a model for the chemical reaction involving SO_2 and water vapor and the eventual production of sulfuric acid H_2SO_4. The description below is intended to be useful as a model for the reaction that occurs when SO_2 invades the pore space of a filter composed of solid carbon (catalyst) particles.

2.1 Assumptions

The derivation that follows is based on two key assumptions.

1. The diffusion is much faster than the reaction.
2. The energy for the oxidation is much larger than that of deactivation of catalyst sites (oxidation 93.55 kJ/kmol, deactivation 21.4 kJ/mol) [5], so the deactivation is faster than the reaction.

Assumption 1 implies that the concentrations are homogenous in each pore. However, chemical concentrations may vary from one pore to the next in the filter and consequently there may be concentration gradients present on the scale of the filter. Assumption 2 implies that the deactivation process occurs before other reactions and impacts the number of active sites of carbon catalysts for reactions later on.

2.2 Catalyst Deactivation

The deactivation process is a chemisorption,

$$SO_2(aq) + \omega \rightleftharpoons \omega{\cdot}SO_2, \tag{1}$$

where ω denotes the carbon catalyst and $SO_2(aq)$ denotes SO_2 in aqueous solutions as molecular form. We use SO_2 for simplicity. Before deactivation, the activity of ω is 1, which means all the active sites are available. After deactivation, some active sites become deactivated, i.e., they cannot catalyze the reaction. We should notice that the deactivation process is a dynamic equilibrium, and the number of $\omega{\cdot}SO_2$ changes if the concentration of SO_2 changes. However, since deactivation is faster than reaction, (1) always reaches equilibrium before we consider reaction.

Suppose we consider a unit volume from now on. By equilibrium, we mean that

$$\frac{dN_{\omega\cdot SO_2}}{dt} = 0 \tag{2}$$

where N_A denotes the number of molecules of substance A.

Suppose the number of initial active sites is N_{ω_0}, the forward reaction rate of (1) is k_{f1} and the backward reaction rate of (1) is k_{b1}. Then,

$$\frac{dN_{\omega\cdot SO_2}}{dt} = k_{f1}N_{SO_2}N_{\omega_0} - k_{b1}N_{\omega\cdot SO_2} = 0$$

So

$$N_{\omega\cdot SO_2} = \alpha_1 N_{SO_2}N_{\omega_0}, \tag{3}$$

where $\alpha_1 = k_{f1}/k_{b1}$. Hence, the number of available active sites is

$$N_{\omega_{act}} = N_{\omega_0} - N_{\omega\cdot SO_2} = N_{\omega_0} - \alpha_1 N_{SO_2}N_{\omega_0} = (1 - \alpha_1 N_{SO_2})N_{\omega_0}$$

2.3 Reaction

The reaction starts with ionization,

$$SO_2 + H_2O \rightleftharpoons H^+ + HSO_3^- \tag{4}$$

Only those active sites can catalyze the reaction below,

$$HSO_3^- + \omega \rightleftharpoons \omega{\cdot}HSO_3^- \tag{5}$$

$$\omega{\cdot}HSO_3^- + \frac{1}{2}O_2 \longrightarrow H^+ + SO_4^{2-} + \omega \tag{6}$$

Note that the number of ω involved in (5) is $N_{\omega_{act}}$, i.e., available active sites.

Similarly to the catalyst deactivation discussion of the previous subsection, the equilibrium (5) yields

$$N_{\omega{\cdot}HSO_3^-} = \alpha_2 N_{HSO_3^-} N_{\omega_{act}}, \tag{7}$$

where $\alpha_2 = k_{f2}/k_{b2}$.

Suppose the reaction rate of (6) is k, then in unit volume,

$$\frac{dN_{SO_4^{2-}}}{dt} = k \cdot N_{\omega HSO_3^-} \cdot N_{O_2}^{\frac{1}{2}}.$$

If we now substitute equation (3) and equation (7) into the expression above, we find

$$\frac{dN_{SO_4^{2-}}}{dt} = k \cdot \alpha_2 \cdot N_{HSO_3^-} \cdot (1 - \alpha_1 N_{SO_2}) \cdot N_{\omega_0} \cdot N_{O_2}^{\frac{1}{2}}.$$

Now we define that the activity of initial catalyst (before deactivation) is 1, which is a very common assumption for pure solid and pure liquid. By definition, the activity is $a = \frac{N_\omega}{N_{\omega_0}}$ in a unit volume, which means N_{ω_0} yields an activity of 1 on the right-hand side.

In the chemical equilibrium equation, we usually use the thermodynamic activities of the chemical species; that is, concentration for gas or substances in solution, activity for liquid and solid (more information see wikipedia [1]). We can convert the number of substances into concentration or activity in the above equation, because we consider a unit volume for all the relations and equations above. So

$$\frac{d\tilde{C}_{SO_4^{2-}}}{dt} = k \cdot \alpha_2 \cdot C_{HSO_3^-} \cdot (1 - \alpha_1 C_{SO_2}) \cdot 1 \cdot C_{O_2}^{\frac{1}{2}}. \tag{8}$$

Here C_A is the concentration ($\text{mol} \cdot \text{m}^{-3}$) of substance A. For ease of notation we have reused the variable names α_1 and α_2 in equation (8) but note here that they now are interpreted as quantities with units $\text{mol}^{-1} \cdot \text{m}^3$ (whereas previously they had units mol^{-1}). The quantity $\tilde{C}_{SO_4^{2-}}$ denotes the SO_4^{2-} produced in equation (6) and is described in more detail below after (9).

The last step of the reaction is

$$SO_4^{2-} + 2H^+ \rightleftharpoons H_2SO_4. \tag{9}$$

[1] https://en.wikipedia.org/wiki/Equilibrium_constant

This is also a statement of dynamic equilibrium and involves the generation of liquid H_2SO_4 (sulfuric acid). Notice that in (9) the number of S(VI)[2] is conserved; that is, this involves a conversion between SO_4^{2-} and H_2SO_4. So

$$\frac{d\tilde{C}_{SO_4^{2-}}}{dt} = \frac{dC_{S(VI)}}{dt}.$$

Here $\frac{d\tilde{C}_{SO_4^{2-}}}{dt}$ in (6) is not the overall rate of change of SO_4^{2-}, noticing that $C_{SO_4^{2-}}$ decreases after (9). The quantity $\tilde{C}_{SO_4^{2-}}$ minus the consumed amount of SO_4^{2-} in equation (9) below would represent the real concentration of SO_4^{2-}. However, in the present context we care more about S(VI), which consists of SO_4^{2-} and H_2SO_4, than we do about the real concentration of SO_4^{2-}. Therefore, since S(VI) is conserved in (9), as an estimate for the rate of change of concentration of S(VI) we use the rate of change of the quantity $\tilde{C}_{SO_4^{2-}}$.

In our project, we are concerned about the rate of change of the volume of liquid, i.e., in a pore (with given void volume),

$$\frac{dV_{H_2SO_4}}{dt} = ?$$

If we assume that (9) arrives at equilibrium much faster than the reaction (6), it implies that there is a $\tilde{K} < 1$ such that, when the total amount of SO_4^{2-} generated in equation (6) is $\tilde{N}_{SO_4^{2-}}$, then $N_{H_2SO_4} = \tilde{K}\tilde{N}_{SO_4^{2-}}$. And we should notice that the amount of SO_4^{2-} after the equilibrium (9) is

$$N_{SO_4^{2-}} = \tilde{N}_{SO_4^{2-}} - N_{H_2SO_4},$$

and by equilibrium,

$$\alpha_3 N_{SO_4^{2-}} N_{H^+}^2 = N_{H_2SO_4},$$

where $\alpha_3 = k_{f3}/k_{b3}$ is the equilibrium constant for (9). Then,

$$\tilde{K} = \frac{\alpha_3 N_{H^+}^2}{1 + \alpha_3 N_{H^+}^2}$$

or, re-using the variable name α_3 with an appropriate unit conversion for concentration,

$$\tilde{K} = \frac{\alpha_3 C_{H^+}^2}{1 + \alpha_3 C_{H^+}^2}$$

considering any volume.

Therefore, the rate of change of sulfuric acid concentration is given by

$$\frac{dC_{H_2SO_4}}{dt} = \tilde{K}\frac{d\tilde{C}_{SO_4^{2-}}}{dt} = \frac{k\alpha_2\alpha_3 C_{H^+}^2}{1 + \alpha_3 C_{H^+}^2} \cdot C_{HSO_3^-} \cdot (1 - \alpha_1 C_{SO_2}) \cdot C_{O_2}^{\frac{1}{2}} \tag{10}$$

[2]S(IV) consists of SO_2 and HSO_3^-. S(VI) consists of SO_4^{2-} and H_2SO_4. [5]

2.4 Liquid Volume Generation

We further analyze equation (10) in order to obtain an equation for the rate of liquid volume generated by the reaction. Since the ratio of SO_2 is considered small in the gas mixture, we can assume that C_{O_2} is constant and C_{H^+} is fixed. The dynamic equilibrium statements in (4) and (9) indicate that

$$\alpha_3 C_{H_2SO_4} C_{H^+}^2 = C_{SO_4^{2-}} \tag{11}$$

$$\alpha_4 C_{SO_2} = C_{H^+} \cdot C_{HSO_3^-} \tag{12}$$

where activity of H_2O in the latter equation is 1. Equation (10) reduces to,

$$\frac{dC_{H_2SO_4}}{dt} = KC_{SO_2}(1 - \alpha_1 C_{SO_2}) \tag{13}$$

where

$$K = \frac{k\alpha_2\alpha_3\alpha_4 C_{H^+}}{(1 + \alpha_3 C_{H^+}^2)} C_{O_2}^{\frac{1}{2}}.$$

To convert concentration C_k of species k to volume V_k of species k, note that two ways to express the mass of species k in the total volume V_t are in terms of mass density and concentration yielding

$$\rho_k V_k = C_k V_v M_k,$$

where ρ_k is the mass density of species k measured in a volume V_k of species k, C_k is the concentration of species k (number of moles per void volume V_v) and M_k is the molecular mass (mass of one mole) of species k. That is, the volume occupied by species k is

$$V_k = \frac{V_v M_k}{\rho_k} C_k,$$

Define saturation (i.e. volume fraction) of liquid and gas phases

$$S^l = \frac{V_{H_2SO_4}}{V_t}, \quad S^g = \frac{V_{SO_2}}{V_t},$$

where the total volume $V_t = V_s + V_v$ is the sum of the solid volume and void volume. To simplify notation we denote the liquid H_2SO_4 by superscript 'l' and gas SO_2 by superscript 'g'. Differentiating V^l with respect to time, using the volume/concentration conversion formulas and equation (13) gives

$$V_t \frac{dS^l}{dt} = \frac{V_v M^l}{\rho^l} \frac{dC^l}{dt} = \frac{V_v M^l}{\rho^l} \cdot K \cdot \frac{\rho^g}{V_v M^g} V_t S^g (1 - \alpha_1 \frac{\rho^g}{V_v M^g} V_t S^g).$$

If we let

$$\alpha = \frac{\alpha_1 V_t \rho^g}{V_v M^g}, \quad \kappa = \frac{\rho^g M^l}{\rho^l M^g} \cdot \frac{k\alpha_2\alpha_3\alpha_4 C_{H^+}}{(1 + \alpha_3 C_{H^+}^2)} C_{O_2}^{\frac{1}{2}},$$

then the liquid volume production can be expressed in terms of the gas saturation S^g

$$\frac{dS^l}{dt} = \kappa S^g (1 - \alpha S^g). \tag{14}$$

This expression reveals a dual role of the presence of SO_2 for the generation of H_2SO_4. First, the presence of SO_2 is required for the reaction to proceed at all; this is represented by the first appearance of the term S^g indicating that without SO_2 there would

be no liquid generation. Second, the SO_2 can bind directly to catalyst sites and reduce the rate at which the reactions (6) and therefore (9), which produces H_2SO_4, can take place. This effect is embodied in the term $(1 - \alpha S^g)$ in equation (14). This process as a whole is schematically shown in Figure 2 in which SO_2 is present in the gas phase, plays a role in the production of HSO_3^- (which promotes H_2SO_4 production), and can bind to and deactivate catalyst sites (which inhibits H_2SO_4 production).

Another key issue that plays a role in the availability of catalyst sites is the distribution of the liquid phase (H_2SO_4) on the catalyst surface. The presence of this liquid phase in contact with the solid particles can also block access to active catalyst sites even if no deactivation of catalyst sites by direct binding of SO_2 takes place. We discuss this fluid-mechanical mechanism further in the next section where we formulate a network-based model for the filter as a whole.

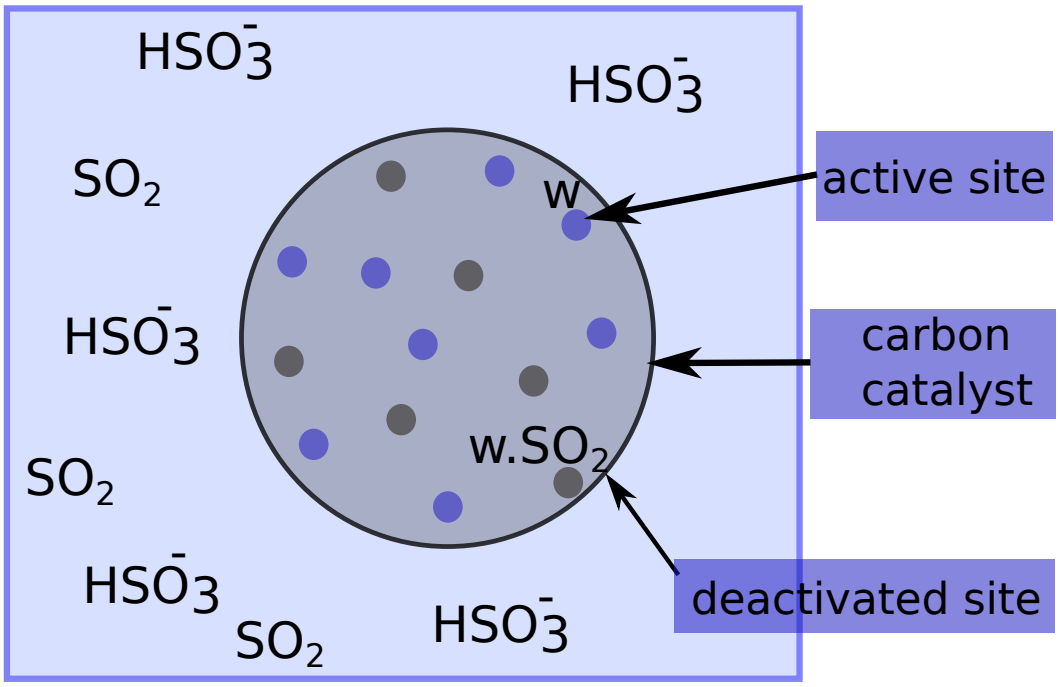

Figure 2: This figure shows some of the key features of the chemical reaction including the dual role of sulfur dioxide (SO_2) in the production of sulfuric acid (H_2SO_4). Sulfur dioxide is present in the gas phase, plays a role in the production of HSO_3^- (which promotes H_2SO_4 production), and can bind to and deactivate catalyst sites (which inhibits H_2SO_4 production).

3 A Two-Dimensional Network Model for the Filter

In this section we now consider a catalyst layer (e.g. the filter) in the form of a packed bed of particles characterized by a network of interconnected pores. The idea of this model is to allow reactant gas exposed to the filter at one exterior boundary to diffuse into the network, react on the particle surface and produce fluid that can partially or completely fill the pore space.

As a model for chemical diffusion of a reactive gas into a two-dimensional porous filter consider a set of N nodes indexed by i representing catalyst particles distributed within a horizontally long and vertically thin rectangular domain. The cross section of the filter to be modeled has a vertical thickness much smaller than its horizontal length. We assume a line of symmetry within the filter representative of a periodic 'stack' of these filters placed in the flow (see Figure 3). A reactive gas flows horizontally along one (long) side of the filter. There is no imposed flow or pressure jump across the filter, however, gas transport by diffusion into the filter is expected to occur. Each node i has associated with it a volume (per unit length) V_i. The volume is made up of a reactive gas volume V_i^g, a non-reactive gas volume V_i^{g2}, a liquid phase volume V_i^l and a solid phase volume V_i^s [the catalyst particle(s)] so that $V_i = V_i^g + V_i^{g2} + V_i^l + V_i^s$. We assume that V_i^s is fixed for a given cell but that the volumes of the other three phases can evolve in time. We work in terms of saturations (or volume fractions) $S_i^g = V_i^g/V_i$, $S_i^{g2} = V_i^{g2}/V_i$, $S_i^l = V_i^l/V_i$ and $S_i^s = V_i^s/V_i$ which have the property $S_i^g + S_i^{g2} + S_i^l + S_i^s = 1$. Of interest in each cell is the liquid volume fraction S_i^l and the reactive gas volume fraction S_i^g. In addition to these quantities we denote the initial area (per unit length) of the solid catalyst in cell i by A_i^s.

An open question in this setting is the description of how the fluid produced by the reaction is distributed within the network. We present one model that assumes that the fluid produced is evenly distributed on the catalyst surface in the form of tiny spherical droplets (capillary static shape) that adhere to the surface with a fixed contact angle. This particular model for fluid distribution within the pore space necessarily becomes invalid at the point at which a sufficient fluid volume is generated for coalescence of the tiny drops to occur (of course coalescence or other fluid distribution configurations may occur even sooner). The volume at which coalescence in this model must occur is predicted as a function of the contact angle. These are described in more detail below.

3.1 Conservation Equations

The following are mass balance equations for cells $i = 1, \ldots, N$ that relate the rate of change of liquid and reactive gas in a given cell to source/sink terms associated with chemical reactions and flux/diffusion from neighboring cells. The model we present here is inspired by the work of Sinha and Wang [6] although they consider a pressure-driven flow from a boundary of the filter and do not incorporate the possibility of a chemical reaction in the pore space. Related network models include those of El Hannach and coworkers [3, 4]. Here we write

$$\rho_l V_i \frac{dS_i^l}{dt} = \kappa S_i^g (1 - \alpha S_i^g) A(S_i^l) + \rho_l \sum_{j \in N_i} Q_{ij}^l, \tag{15}$$

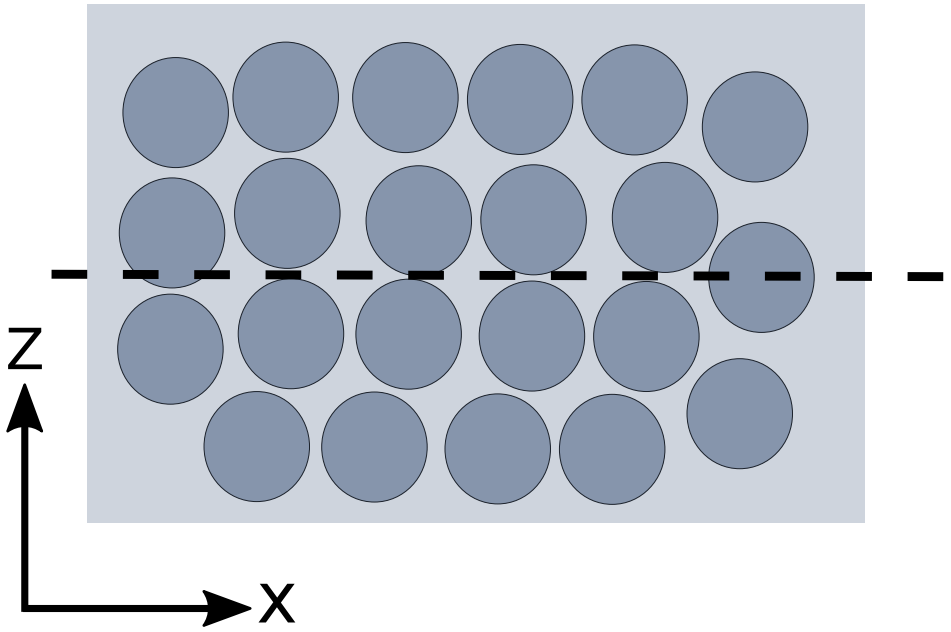

Figure 3: This figure shows a sketch of the cross-section of particles in the network model. Each pore can be thought of as representing a volume V_i composed of solid, liquid and gas phases. Connectivity of one pore to the next can be specified in a computational setting. For simplicity in the present work we consider pores on a regular grid with nearest-neighbor coupling.

$$\rho_g V_i \frac{dS_i^g}{dt} = -\sum_{j \in N_i} \mathcal{D}(S_i^g - S_j^g) - \kappa S_i^g (1 - \alpha S_i^g) A(S_i^l), \tag{16}$$

where ρ_l is the density of the liquid phase, ρ_g is the density of the reactive gas phase, κ is a rate constant that characterizes the reaction in which the reactive gas is consumed and liquid is produced [see equation (14)], $A(S_i^l)$ is the available area of catalyst which we assume is a function of the amount of liquid present in the cell and how it this

liquid is distributed throughout the cell (we discuss possible models for this quantity below), Q_{ij}^l represents the volume flux of liquid into cell i from the neighboring cells j whose indices are denoted by N_i (we discuss possible models for Q_{ij}^l below) and $\mathcal{D}$ is a diffusion coefficient, which we assume for simplicity to be a constant. In the continuum model section that follows, we shall allow the diffusion coefficient to vary with the amount of liquid present. In the first equation, the liquid content in a given cell may change due to the production of liquid from the reaction (which requires the presence of the reactive gas and available catalyst surface area) and transfer of liquid to/from neighboring cells. In the second equation the change of reactive gas volume fraction in a cell is determined by diffusion of gas to/from neighboring cells and the consumption of gas from the reaction. Note that the solid volume fraction in each cell, S_i^s, is given initially and remains constant for all time and the non-reactive gas volume fraction can be determined from the condition $S_i^g + S_i^{g2} + S_i^l + S_i^s = 1$ once the ODEs for S_i^l and S_i^g are solved. In order to close this model we need to specify models for the exposed solid area $A(S_i^l)$ and the fluxes from the neighboring cells Q_{ij}^l.

For initial conditions, we shall assume that initially all cells contain no liquid so that $S_i^l = 0$ at time zero. Also, all cells that are not at the bottom of the filter have $S_i^g = 0$. Those cells at the bottom of the filter exposed to the reactive gas flow have $S_i^g = 1 - S_i^s$. The present network model is not coupled to dynamics occurring in an adjacent channel (other than through the prescription of S_i^g in the boundary cells). In principle, however, one could couple this network model to a chemical transport model in the channel. We discuss such a model in the context of a continuum formulation in more detail in later sections. In the computational model here a symmetry condition (no flux) condition is imposed at the upper boundary of the computational domain representing the center line of the filter.

3.2 Models for Fluxes from Neighbors and Cell Pressure

A model for Q_{ij}^l, the transfer of fluid from neighboring cell j to cell i in general must be determined. The model proposed by Sinha & Wang [6] – see their equations (6), (7) and (8) – is based on the idea that a pressure is imposed at one boundary of their system and so the fluid motion is driven by this external pressure. In our system we have fluid generated within the system and no pressure gradient (pressure differences between adjacent cells) to drive flow. The fluid phase redistributes, it would seem, based on mass conservation principle, coupled in some way to capillary statics of fluid filling void space created by hydrophobic particles. The quasi-static fluid invasion problem is beyond the scope and constraints of the present study but has been addressed in the literature (e.g. Cieplak & Robbins[2]).

A starting point that serves the purpose of describing early time behavior, before a sufficient amount of fluid for transfer between cells is generated, is to consider the case $Q_{ij}^l = 0$. The behavior of the system with $Q_{ij}^l = 0$ will serve as a basis for comparison once a suitable model for Q_{ij}^l is obtained.

3.3 Models for Available Area on Catalyst

The production of liquid in the chemical reaction requires that one address models of how this liquid is distributed in each cell. In the sections that follow we describe

possible models that relate the available surface area of catalyst to the volume fraction of liquid S_i^l inside the cell.

3.3.1 Tiny Droplets form Uniformly on Catalyst Surface

Here we assume that the catalyst is hydrophobic so that at least for early times liquid generated from the reaction distributes itself uniformly over the surface area A_i^s of the cell in the form of small spherical-cap shaped droplets. If we assume that the surface area of the catalyst A_i^s can be subdivided into $w \times w$ rectangular patches then the number of such patches covering the surface of the catalyst is $N_{patch} = A_i^s/w^2$. We assume that as liquid is produced at the surface of the catalyst it is distributed in the form of a single liquid drop on each the the N_{patch} patches. Each drop has a fixed contact angle θ with respect to the substrate surface and a volume V_{drop} that can evolve in time. We assume this configuration can be applied up to the point at which droplet coalescence occurs through contact of neighboring droplets. At the end of this section we compute the maximum droplet volume allowed before coalescence occurs and show how this volume depends on the contact angle. Assuming such a distribution of liquid in the form of tiny droplets on the surface of the catalyst we can relate the volume fraction of liquid in the entire cell to the volume of an individual droplet

$$S_i^l = \frac{N_{patch} V_{drop}}{V_i} = \frac{A_i^s}{V_i w^2} V_{drop}. \tag{17}$$

Our objective below is to relate the catalyst surface area covered by a single droplet to V_{drop} and the contact angle θ. Then, summing each covered area over all the drops and subtracting the result from the total solid surface area A_i^s gives the available catalyst surface area $A(S_i^l)$. We describe this procedure below.

Consider a planar surface subdivided into square grids of size $w \times w$. Suppose a liquid droplet of volume V_{drop} is attached at the center of each of these squares. Assuming the shape of this liquid droplet is determined by surface tension, the droplet will have constant curvature and will take the form of a spherical cap. Denote by H the height of the drop and R the radius of the droplet (i.e. the radius of the corresponding sphere). The volume of this spherical cap is $\frac{1}{3}\pi H^2(3R - H)$. If we assume that the droplet makes a contact angle $\theta \in [0, \pi]$ with respect to this horizontal surface we can express the volume of the droplet as

$$V_{drop} = \frac{\pi R^3}{3} \left(1 - \cos\theta\right)^2 \left(2 + \cos\theta\right). \tag{18}$$

This droplet makes a circular contact with the substrate. If we denote by W the radius of this circular contact we have

$$\cos(\theta - \pi/2) = \sin\theta = \frac{W}{R}, \quad \sin(\theta - \pi/2) = -\cos\theta = \frac{H - R}{R}. \tag{19}$$

It follows that the contact area can be expressed as

$$\begin{aligned} A_{contact} &= \pi W^2, \\ &= \pi R^2 \sin^2\theta, \\ &= \pi \left(\frac{3V_{drop}}{\pi}\right)^{\frac{2}{3}} \left(\frac{\sin^3\theta}{(1 - \cos\theta)^2(2 + \cos\theta)}\right)^{\frac{2}{3}} \end{aligned} \tag{20}$$

If we now convert this to a total available area for reaction by subtracting from the original solid surface area, A_i^s, the area covered by all N_{patch} drops whose contact surface area is $A_{contact}$ we find that

$$\begin{aligned} A(S_i^l) &= A_i^s - \frac{A_i^s}{w^2} A_{contact}, \\ &= A_i^s - \frac{A_i^s}{w^2}\pi \left(\frac{3V_{drop}}{\pi}\right)^{\frac{2}{3}} \left(\frac{\sin^3\theta}{(1-\cos\theta)^2(2+\cos\theta)}\right)^{\frac{2}{3}}, \qquad (21) \\ &= A_i^s - \frac{A_i^s}{w^2}\pi \left(\frac{3S_i^l w^2 V_i}{\pi A_i^s}\right)^{\frac{2}{3}} \left(\frac{\sin^3\theta}{(1-\cos\theta)^2(2+\cos\theta)}\right)^{\frac{2}{3}}, \qquad (22) \\ &= A_i^s \left[1 - \pi \left(\frac{3S_i^l V_i}{\pi A_i^s w}\right)^{\frac{2}{3}} \left(\frac{\sin^3\theta}{(1-\cos\theta)^2(2+\cos\theta)}\right)^{\frac{2}{3}}\right], \qquad (23) \\ &= A_i^s \left[1 - f(\gamma_i,\theta)(S_i^l)^{\frac{2}{3}}\right], \qquad (24) \end{aligned}$$

where we have used the result $V_{drop} = S_i^l w^2 V_i / A_i^s$ from equation (17) and we have defined

$$f(\gamma_i,\theta) = \pi \left(\frac{3\gamma_i}{\pi}\right)^{\frac{2}{3}} \left(\frac{\sin^3\theta}{(1-\cos\theta)^2(2+\cos\theta)}\right)^{\frac{2}{3}}, \qquad (25)$$

where $\gamma_i = V_i/(wA_i^s)$.

In this scenario, there is a limit to the total volume of fluid that can be distributed on a surface in the form of tiny droplets before they grow too large and coalesce in some way. We can predict the critical volume for which this occurs. There are two cases that one must consider here in terms of the contact angle depending on whether the contact angle is greater than or less than $\pi/2$.

First, if $\theta > \pi/2$ the widest point on the droplet occurs some distance above the substrate. In this case, coalescence occurs when the droplet radius R meets or exceeds $w/2$. We therefore define a critical droplet volume V_c as the maximum drop volume that can be remain isolated from its neighbors on a uniform $w \times w$ grid

$$V_{drop}^c = \frac{\pi w^3}{24}(1-\cos\theta)^2(2+\cos\theta) \qquad \text{for } \theta > \pi/2 \qquad (26)$$

Second, if $\theta < \pi/2$ the widest point on the droplet occurs at the substrate. In this case, coalescence occurs when the droplet contact width W meets or exceeds $w/2$. Recall that the droplet radius R is related to W through $W = R\sin\theta$. So, when $W = w/2$ we have that $R = w/(2\sin\theta)$. Therefore, the critical droplet volume (maximum drop volume before coalescence) is

$$V_{drop}^c = \frac{\pi w^3}{24}\frac{(1-\cos\theta)^2(2+\cos\theta)}{\sin^3\theta} \qquad \text{for } \theta \le \pi/2. \qquad (27)$$

Figure 4 shows a scaled droplet volume $24V_{drop}^c/(\pi w^3)$ as a function of contact angle θ indicating that droplets with smaller contact angles will coalesce at smaller volumes as compared to droplets with large contact angle. It follows that this model for $A(S_i^l)$ is only applicable as long as

$$S_i^l \le \frac{A_i^s}{V_i w^2} V_{drop}^c = \mathcal{O}\left(\frac{A_i^s w}{V_i}\right). \qquad (28)$$

If we suppose that a typical pore is cubic with volume X^3 and that the catalyst particle has approximately those same dimensions so that $A_i^s \sim X^2$, then the formula given above would suggest that the upper limit for liquid volume scales with w/X which we expect to be quite small (spacing between catalyst sites relative to a typical particle length scale). It would seem that this particular model for liquid distribution in the pore space may not be valid for volumes of interest for phenomena such as flooding.

3.3.2 One Big Droplet Forms on Catalyst Surface

Another possible distribution of fluid within the cell corresponds to the volume of fluid produced forming a solitary droplet that adheres to the catalyst surface with contact angle θ. We have not calculated the resultant form of $A(S_i^l)$ here but anticipate that it has the property that the area monotonically decreases with S_i^l.

3.3.3 Liquid Forms but Detaches from Catalyst Surface

Here $A(S_i^l) = A_i^s$. That is, the available surface area is the original surface area and remains constant despite formation of liquid. Presumably this is an idealized case and may be useful as a reference case for understanding/interpreting other models for $A(S_i^l)$. This would somehow be the best case scenario – namely, liquid forms but does not reduce the available surface area for reaction and consumption of SO_2. Note that the formation of liquid would tend to reduce the volume fraction of reactive gas S_i^g and so in that way may indirectly inhibit the reaction. Eventually this model would break down as there is only a limited amount of pore space within each cell and given a sufficient volume of fluid the catalyst surface must become engulfed by the fluid. The issue of reduction of diffusion pathways as more liquid forms must also be addressed. We discuss this to some degree in the context of the continuum approach.

3.4 Preliminary Numerical Results of the Network Model

A two-dimensional pore network was set up on a rectangular grid to simulate the gas saturation (SO_2) and liquid saturation in the model filter. Pore properties were uniform throughout the filter. A preliminary calculation is shown in Figure 5. Here the filter is exposed to a high concentration of SO_2 at the bottom boundary. Diffusion through the filter pore space can be observed in the upper figure. The liquid saturation, resulting from the chemical interaction of the SO_2 with the catalyst sites, is shown and follows the SO_2 saturation. This model is not coupled to the gas flow in the channel (exterior to the filter), however, one could in principle compute the flux of SO_2 into the filter as a means of estimating the efficiency of the filter in removing SO_2 from the surrounding environment. An avenue worthy of exploration in the present model is the incorporation of pore size distribution in the filter. Optimization of the pore size distribution may offer new insights for filter design.

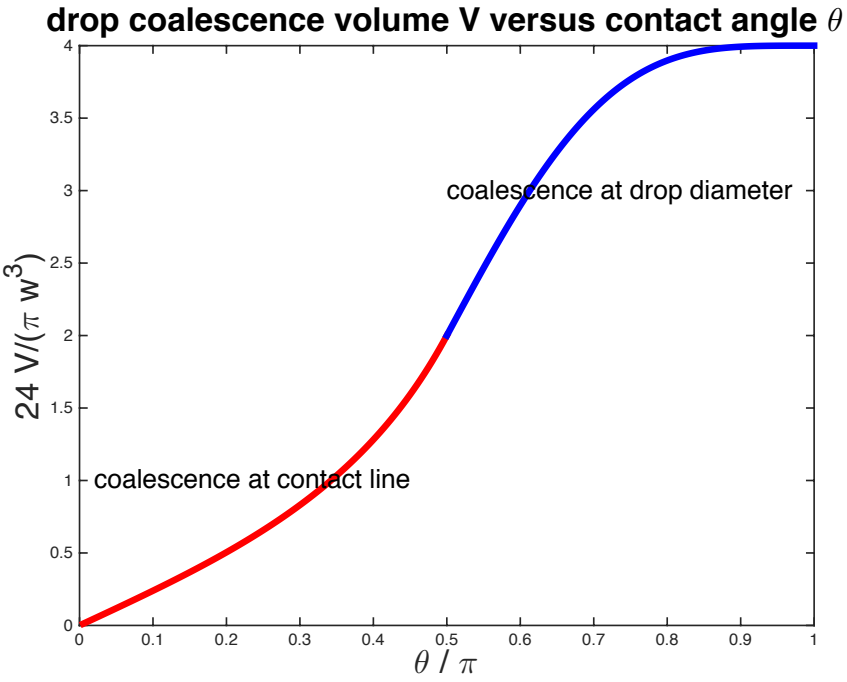

Figure 4: Dimensionless droplet coalescence volume as a function of contact angle assuming an array of droplets of distributed on a rectangular $w \times w$ grid. Droplets with smaller contact angles coalesce at smaller volumes while droplets with larger contact angles coalesce at larger volumes.

4 Two-Dimensional Continuum Filter/Channel Model

Here we consider the transport of reactive gas (SO_2) through the open channels between an array of porous filters and the subsequent chemical reaction and fluid generation

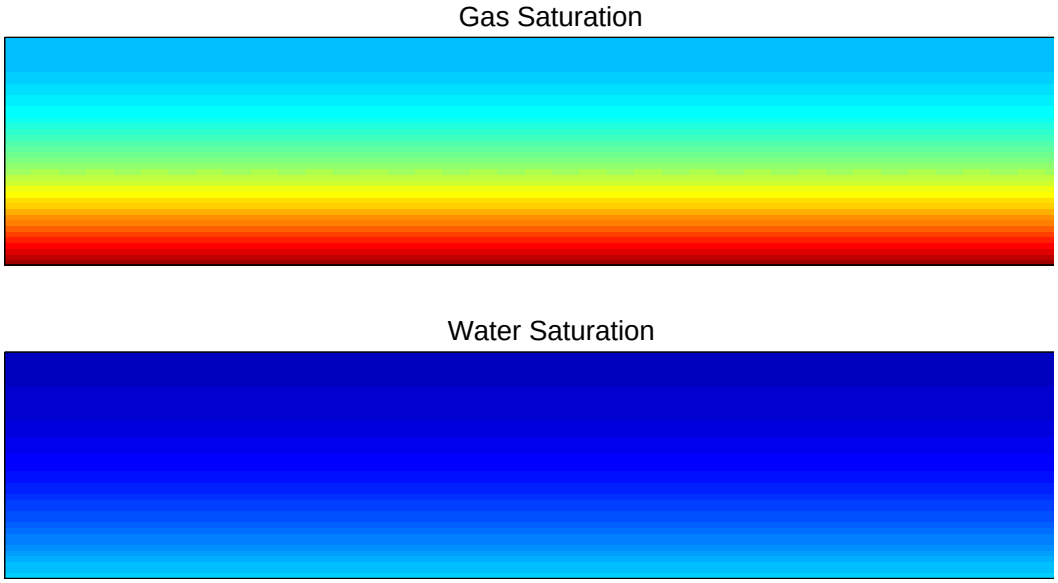

Figure 5: This figure shows a preliminary result from the network model. In the upper plot the saturation of SO_2 is shown with higher values at the bottom near the boundary exposed to the channel flow. In the lower plot the liquid saturation is shown to follow the SO_2 saturation.

within the filters. Numerical solutions of the model allow one to predict (1) the reduction in total amount of SO_2 at the channel exit compared to the channel inlet and (2) the time evolution and spatial distribution of fluid generation and SO_2 concentration within the filter. The model is based on a continuum multi-species/multi-phase characterization of the filter as a porous medium.

4.1 Transport Theorem

It is useful to recall the transport theorem applied to a scalar quantity ψ defined on a time-dependent volume $\Omega(t)$, which states that

$$\frac{d}{dt}\int_{\Omega(t)} \psi dV \quad = \quad \int_{\Omega(t)} \left[\frac{\partial \psi}{\partial t} + \nabla \cdot (\psi \vec{w})\right] dV, \tag{29}$$

where $\vec{w}$ is the speed of displacement of the surface of $\Omega(t)$.

4.2 Conservation Equations for Multiphase System

We consider a fixed control volume Ω of a multiphase system that contains a representative sample of solid, liquid and gas phases. We denote the volume of Ω by V_Ω which is divided up into volume occupied by the solid, V_Ω^s, volume occupied by the liquid, V_Ω^ℓ and volume occupied by the gas V_Ω^g. In the present continuum model we denote volume fractions (or saturations) of each phase by $\phi_s = V_\Omega^s/V_\Omega$, $\phi_\ell = V_\Omega^\ell/V_\Omega$ and $\phi_g = V_\Omega^g/V_\Omega$. As in a standard continuum description, we treat these volume fractions as defined at each point in space and time. It follows that everywhere in the system

$$\phi_s + \phi_\ell + \phi_g \quad = \quad 1. \tag{30}$$

Global balances for solid, liquid and gas state that the rate of change of mass of a particular phase in Ω is equal to the net mass flux of that phase through the boundary plus the total production (or consumption) of the phase due to chemical reaction and/or phase transformation

$$\frac{d}{dt}\int_\Omega \rho_s \phi_s dV \quad = \quad -\int_{\partial\Omega} \vec{J}_s^{\,0} \cdot \hat{n} dS + \int_\Omega \dot{R}_s^{prod} dV, \tag{31}$$

$$\frac{d}{dt}\int_\Omega \rho_\ell \phi_\ell dV \quad = \quad -\int_{\partial\Omega} \vec{J}_\ell^{\,0} \cdot \hat{n} dS + \int_\Omega \dot{R}_\ell^{prod} dV, \tag{32}$$

$$\frac{d}{dt}\int_\Omega \rho_g \phi_g dV \quad = \quad -\int_{\partial\Omega} \vec{J}_g^{\,0} \cdot \hat{n} dS + \int_\Omega \dot{R}_g^{prod} dV. \tag{33}$$

Here ρ_ℓ, ρ_s and ρ_g are mass densities of the liquid, solid and gas phases, respectively. The mass fluxes for solid, liquid and gas phases are

$$\vec{J}_s^{\,0} = \rho_s \phi_s \vec{u}_s, \quad \vec{J}_\ell^{\,0} = \rho_\ell \phi_\ell \vec{u}_\ell, \quad \vec{J}_g^{\,0} = \rho_g \phi_g \vec{u}_g, \tag{34}$$

where $\vec{u}_s$, $\vec{u}_\ell$ and $\vec{u}_g$ are local velocities of the solid, liquid and gas phases, respectively. The reaction terms $\dot{R}_s^{prod}$, $\dot{R}_\ell^{prod}$ and $\dot{R}_g^{prod}$ represent production rates (or consumption) of mass of a particular phase per unit volume due to chemical reaction or phase transformation. Note that the reaction terms can be interpreted as redistributing mass from one phase to another. For example, if we have a reaction that converts a certain mass of gas to the same mass of liquid with no creation/consumption of the solid phase then $\dot{R}_s^{prod} = 0$ and $\dot{R}_g^{prod} + \dot{R}_\ell^{prod} = 0$.

In the general case, summing the global balances (31)–(33), applying the transport theorem (noting that the boundary of Ω is fixed) and using the divergence theorem on the surface integrals gives

$$\int_\Omega \left[\frac{\partial \rho}{\partial t} + \nabla \cdot (\rho \vec{u})\right] dV \quad = \quad \int_\Omega \left(\dot{R}_s^{prod} + \dot{R}_\ell^{prod} + \dot{R}_g^{prod}\right) dV \tag{35}$$

where $\rho = \rho_s\phi_s + \rho_\ell\phi_\ell + \rho_g\phi_g$ is the total mass density and $\vec{u}$ is the barycentric (mass-averaged) velocity defined by $\rho\vec{u} = \rho_s\phi_s\vec{u}_s + \rho_\ell\phi_\ell\vec{u}_\ell + \rho_g\phi_g\vec{u}_g$. By conservation of total mass we must have $\dot{R}_s^{prod} + \dot{R}_\ell^{prod} + \dot{R}_g^{prod} = 0$. Therefore, recognizing that the control volume Ω is arbitrary leads to the local statement of mass conservation

$$\frac{\partial\rho}{\partial t} + \nabla\cdot(\rho\vec{u}) \;=\; 0. \tag{36}$$

One can also express the mass fluxes relative to the barycentric velocity in the form

$$\vec{J}_s^{\,0} = \rho_s\phi_s\vec{u} + \vec{J}_s^{\,B}, \quad \vec{J}_\ell^{\,0} = \rho_\ell\phi_\ell\vec{u} + \vec{J}_\ell^{\,B}, \quad \vec{J}_g^{\,0} = \rho_g\phi_g\vec{u} + \vec{J}_g^{\,B}, \tag{37}$$

where $\vec{J}_s^{\,B} = \rho_s\phi_s(\vec{u}_s - \vec{u})$ (and similarly for liquid and gas) is the molecular mass flux specified with respect to the barycentric frame. Individual local mass balances for solid, liquid and gas phases are

$$\frac{\partial(\rho_s\phi_s)}{\partial t} + \nabla\cdot(\rho_s\phi_s\vec{u}) \;=\; -\nabla\cdot\vec{J}_s^{\,B} + \dot{R}_s^{prod}, \tag{38}$$

$$\frac{\partial(\rho_\ell\phi_\ell)}{\partial t} + \nabla\cdot(\rho_\ell\phi_\ell\vec{u}) \;=\; -\nabla\cdot\vec{J}_\ell^{\,B} + \dot{R}_\ell^{prod}, \tag{39}$$

$$\frac{\partial(\rho_g\phi_g)}{\partial t} + \nabla\cdot(\rho_g\phi_g\vec{u}) \;=\; -\nabla\cdot\vec{J}_g^{\,B} + \dot{R}_g^{prod}. \tag{40}$$

For a closely related discussion see the textbook by Bird, Stewart and Lightfoot [1], Chapter 19. Two special cases of the continuity equation (36) are discussed below.

- **Solid–Liquid System with Freezing/Melting:** Suppose $\phi_g = 0$ so only solid and liquid phases are present. Then $\phi_\ell = 1 - \phi_s$. Further assume that ρ_s and ρ_ℓ are constants and that the solid phase is rigid so $\vec{u}_s = 0$. Solidification or melting indicates $\partial\phi_s/\partial t \neq 0$. It follows from the continuity equation (36) that

$$(\rho_s - \rho_\ell)\frac{\partial\phi_s}{\partial t} + \rho_\ell\nabla\cdot(\phi_\ell\vec{u}_\ell) = 0. \tag{41}$$

  If we write $\vec{U} = \phi_\ell\vec{u}_\ell$ as is standard in the description of fluid flow in porous media where $\vec{U}$ is the Darcy velocity (volume flux) it follows that

$$\nabla\cdot\vec{U} \;=\; \left(1 - \frac{\rho_s}{\rho_\ell}\right)\frac{\partial\phi_s}{\partial t}. \tag{42}$$

  This equation indicates that there is a nonzero divergence of the flow that is generated from a change of phase if the solid and liquid densities are different. This situation occurs during the solidification of alloys when mushy layers form [7, 8].

- **Gas → Liquid Reaction in a Rigid, Nonreactive Solid Matrix:** This example is more closely related to the present problem of a gas/liquid chemical reaction in a rigid porous medium. Here we have a constant solid fraction ϕ_s and no motion of the solid $\vec{u}_s = 0$. Then $\partial\phi_g/\partial t + \partial\phi_\ell/\partial t = 0$. We assume constant densities of each phase. The continuity equation (36) in this case reduces to

$$\nabla\cdot(\rho_\ell\phi_\ell\vec{u}_\ell + \rho_g\phi_g\vec{u}_g) \;=\; -(\rho_\ell - \rho_g)\frac{\partial\phi_\ell}{\partial t}. \tag{43}$$

If one assumes that the creation of liquid from gas occurs with negligible motion of liquid but a sufficient supply (motion) of gas it follows that

$$\nabla \cdot (\phi_g \vec{u}_g) \quad = \quad -\frac{\rho_\ell}{\rho_g}\left(1 - \frac{\rho_g}{\rho_\ell}\right)\frac{\partial \phi_\ell}{\partial t} \approx -\frac{\rho_\ell}{\rho_g}\frac{\partial \phi_\ell}{\partial t}, \tag{44}$$

where the last approximation follows if the gas phase is much less dense than the liquid phase. Under the stated assumptions, this equation shows that when the fluid phase is generated (e.g. by chemical reaction) there is a sink-like flow of the gas that occurs on a time scale associated with the liquid phase production amplified by the liquid to gas density ratio.

4.3 Conservation Equations - Filter

For the particular case of a porous filter in which gas carrying a certain concentration of sulfur dioxide (SO_2) can react in the presence of the carbon solid catalyst to produce a liquid phase we can use the formalism described in the previous section with an additional balance for the sulfur dioxide species in the gas phase as described in more detail below. In this particular case the solid phase is assumed fixed in space and other than acting as a catalyst for reaction is neither generated or consumed. Hence the mass balance for the solid phase is identically satisfied [i.e. $\rho_s \phi_s$ is time-independent, $\vec{u}_s = 0$ (solid is rigid) and $\dot{R}_s^{prod} = 0$ (solid is non-reactive)]. Local liquid and gas mass balances are

$$\frac{\partial(\rho_\ell \phi_\ell)}{\partial t} + \nabla \cdot (\rho_\ell \phi_\ell \vec{u}) \quad = \quad -\nabla \cdot \vec{J}_\ell^{\mathcal{B}} + \dot{R}_\ell^{prod}, \tag{45}$$

$$\frac{\partial(\rho_g \phi_g)}{\partial t} + \nabla \cdot (\rho_g \phi_g \vec{u}) \quad = \quad -\nabla \cdot \vec{J}_g^{\mathcal{B}} - \dot{R}_\ell^{prod}, \tag{46}$$

where we have used $\dot{R}_\ell^{prod} + \dot{R}_g^{prod} = 0$. As shown in the previous section, the continuity equation follows as a consequence of the local individual balances for the phases. Therefore, we can replace the gas mass balance with the continuity equation

$$\nabla \cdot (\rho \vec{u}) = \nabla \cdot (\rho_\ell \phi_\ell \vec{u}_\ell + \rho_g \phi_g \vec{u}_g) \quad = \quad -(\rho_\ell - \rho_g)\frac{\partial \phi_\ell}{\partial t}. \tag{47}$$

In the present system we are interested in keeping track of the species SO_2, which we assume may be dissolved in the gas phase but is not present in either the liquid or solid phase. Applying similar ideas as formulated in the previous section, we have the global balance stating that the total amount of SO_2 in the control volume Ω changes due to a net mass flux in/out of the domain measured at the domain boundary and by production (or consumption) of SO_2 by chemical reaction within the volume. In particular,

$$\frac{d}{dt}\int_\Omega M_{SO_2} C_{SO_2} \phi_g dV \quad = \quad -\int_{\partial\Omega} \vec{J}^0_{SO_2} \cdot \hat{n} dS + \int_\Omega \dot{R}^{prod}_{SO_2} dV, \tag{48}$$

where M_{SO_2} is the molecular mass of SO_2, C_{SO_2} is the concentration (moles per unit volume) of SO_2, $\vec{J}^0_{SO_2} = M_{SO_2} C_{SO_2} \vec{u} + \vec{J}^{\mathcal{B}}_{SO_2}$ and $\dot{R}^{prod}_{SO_2}$ is the rate of SO_2

mass production per unit volume of gas. The corresponding local species balance is, assuming constant molecular mass M_{SO_2},

$$\frac{\partial(C_{\mathrm{SO}_2}\phi_g)}{\partial t} + \nabla\cdot\left(C_{\mathrm{SO}_2}\phi_g\vec{u}\right) = -\frac{1}{M_{\mathrm{SO}_2}}\nabla\cdot\vec{J}^{\mathcal{B}}_{\mathrm{SO}_2} + \frac{\dot{R}^{prod}_{\mathrm{SO}_2}}{M_{\mathrm{SO}_2}}. \tag{49}$$

4.3.1 Summary of Filter Equations

In summary, the governing equations in the filter are

$$\frac{\partial\phi_\ell}{\partial t} + \nabla\cdot(\phi_\ell\vec{u}) = -\frac{1}{\rho_\ell}\nabla\cdot\vec{J}^{\mathcal{B}}_\ell + \frac{1}{\rho_\ell}\dot{R}^{prod}_\ell, \tag{50}$$

$$\frac{1}{\rho_\ell}\nabla\cdot(\rho\vec{u}) = \nabla\cdot\left(\phi_\ell\vec{u}_\ell + \frac{\rho_g}{\rho_\ell}\phi_g\vec{u}_g\right) = -\left(1-\frac{\rho_g}{\rho_\ell}\right)\frac{\partial\phi_\ell}{\partial t}, \tag{51}$$

$$\frac{\partial(C_{\mathrm{SO}_2}\phi_g)}{\partial t} + \nabla\cdot\left(C_{\mathrm{SO}_2}\phi_g\vec{u}\right) = -\frac{1}{M_{\mathrm{SO}_2}}\nabla\cdot\vec{J}^{\mathcal{B}}_{\mathrm{SO}_2} - \frac{\dot{R}^{prod}_\ell}{M_{\mathrm{SO}_2}}. \tag{52}$$

where $\phi_g = 1-\phi_s-\phi_\ell$. Here we have made the assumption that the production of liquid results from the consumption of an equal mass of SO_2 and so $\dot{R}^{prod}_{\mathrm{SO}_2} = \dot{R}^{prod}_g = -\dot{R}^{prod}_\ell$. Once the fluxes $\vec{J}^{\mathcal{B}}_\ell$ and $\vec{J}^{\mathcal{B}}_{\mathrm{SO}_2}$ along with the chemical reaction rate term $\dot{R}^{prod}_\ell$ are specified, the three equations given here involve the unknown liquid volume fraction ϕ_ℓ, the barycentric velocity $\vec{u}$ and the sulfur dioxide concentration C_{SO_2}. Further information must be provided to determine the velocity $\vec{u}$.

The chemistry outlined earlier and the result in equation (14) suggests the following plausible model for reaction term:

$$\dot{R}^{prod}_\ell = kC_{\mathrm{SO}_2}\left(1-\alpha C_{\mathrm{SO}_2}\right)A(\phi_\ell), \tag{53}$$

where k is a rate constant, the term $1-\alpha C_{\mathrm{SO}_2}$ represents the effect of sulfur dioxide that directly binds to catalyst sites and as a consequence inhibits the reaction that produces the liquid (sulfuric acid) and $A(\phi_\ell)$ is the available area for the reaction whose dependence on the liquid fraction ϕ_ℓ suggests another mechanism that may inhibit the reaction – namely, the build up of liquid on the solid catalysts directly blocking access to the catalyst sites on the solid. Possible models for $A(\phi_\ell)$ were discussed previously. As $\dot{R}^{prod}_\ell$ has units of mass/(time $\times$ volume), C_{SO_2} has units of moles of SO_2 per unit volume and $A(\phi_\ell)$ has units of area the reaction constant k must have units of mass/(mole $\times$ time $\times$ area). The constant α has units of volume per mole.

For the molecular mass flux $\vec{J}^{\mathcal{B}}_{\mathrm{SO}_2}$ we assume Fickian diffusion through the gas phase and liquid phases (no diffusion through the solid)

$$\vec{J}^{\mathcal{B}}_{\mathrm{SO}_2} = -(D_\ell\phi_\ell + D_g\phi_g)\nabla C_{\mathrm{SO}_2}, \tag{54}$$

where $D_\ell \ll D_g$ for the case that diffusion through the liquid phase is much slower than diffusion through the gas phase. Using $\phi_g = 1-\phi_s-\phi_\ell$ it follows that

$$\vec{J}^{\mathcal{B}}_{\mathrm{SO}_2} = -D_g(\frac{D_\ell}{D_g}\phi_\ell + 1 - \phi_s - \phi_\ell)\nabla C_{\mathrm{SO}_2}, \tag{55}$$

$$= -D_g\left[(1-\phi_s) - \left(1-\frac{D_\ell}{D_g}\right)\phi_\ell\right]\nabla C_{\mathrm{SO}_2}, \tag{56}$$

$$= -D_g D_{eff}(\phi_\ell)\nabla C_{\mathrm{SO}_2}, \tag{57}$$

where $D_{eff}(\phi_\ell) = (1-\phi_s) - D\phi_\ell$ and $D \equiv 1 - D_\ell/D_g$. Note that $D \approx 1$ if $D_\ell \ll D_g$. In fact, our previous assumption that the liquid phase carries no amount of SO_2 would suggest that we should use $D = 1$.

4.3.2 A Possible First Model for Transport in the Filter

As a possible first model to explore, consider the following simplifications of the filter model summarized in the previous section. In the liquid fraction equation we assume that the rate of change of liquid volume is dominated by the reaction term with the advection and molecular mass transport negligible. We next assume that the diffusion of sulfur dioxide is rapid (quasi static) but is balanced by the reaction term generating liquid. With these assumptions, the velocity $\vec{u}$ decouples and the equations governing the liquid volume fraction and concentration of sulfur dioxide in the filter are

$$\frac{\partial \phi_\ell}{\partial t} = \frac{k}{\rho_\ell} C_{SO_2}\left(1 - \alpha C_{SO_2}\right) A(\phi_\ell), \tag{58}$$

$$0 = -D_g \nabla \cdot \left(D_{eff}(\phi_\ell)\nabla C_{SO_2}\right) + k C_{SO_2}\left(1 - \alpha C_{SO_2}\right) A(\phi_\ell). \tag{59}$$

4.4 Transport in the Channel Between Filters

A periodic array of filters of length L and thickness $2h$ are assumed to be spaced a distance $2H$ apart. We denote x as the direction along the filter and z the coordinate orthogonal to the filter. Although in reality the filters have finite length in the third direction y we assume that we can model the process in a two-dimensional setting with no variation in the y direction. As such the filter occupies the region $0 < x < L$ and $0 < z < 2h$ although with symmetry conditions we need only to consider the values $0 < z < h$. The space between the filters is represented by $0 < x < L$ and $-2H < z < 0$ where H is half the distance between filters. Again by symmetry we need only to consider the values $-H < z < 0$.

Between the filters, which we denote as the channel, $0 < x < L$ and $-H < z < 0$ sulfur dioxide is transported by advection and diffusion

$$\frac{\partial C_{SO_2}}{\partial t} + \nabla \cdot \left(C_{SO_2}\vec{u}_{chan}\right) = \frac{D_g}{M_{SO_2}} \nabla^2 C_{SO_2}. \tag{60}$$

For simplicity we shall assume that $\vec{u}_{chan} = (u_c, 0, 0)$ is a given constant corresponding to parallel plug flow although different assumptions in which it is determined by a full Navier-Stokes simulation or a more simplified Poiseuille-type parallel flow assumption in which it may depend on the z coordinate are possible. Upon entry to the channel we assume that the concentration of sulfur dioxide is known $C_{SO_2}(x=0) = C^{in}_{SO_2}$. At the channel–filter boundary we have the following boundary conditions

$$C_{SO_2}(z = 0^-) = C_{SO_2}(z = 0^+), \tag{61}$$

$$\left.\frac{\partial C_{SO_2}}{\partial z}\right|_{z=0^-} = D_{eff}(\phi_\ell)\left.\frac{\partial C_{SO_2}}{\partial z}\right|_{z=0^+}, \tag{62}$$

which represent continuity of species and species flux.

4.5 A Possible First Model for Transport in the Channel

As a possible first model to explore and couple to the filter transport, consider the situation in which the concentration of sulfur dioxide in the channel is quasi-static with the transport dominated by advection along the channel (in the x direction) and diffusion in the cross-stream (z) direction. That is,

$$u_c \frac{\partial C_{\mathrm{SO}_2}}{\partial x} = \frac{D_g}{M_{\mathrm{SO}_2}} \nabla^2 C_{\mathrm{SO}_2}. \tag{63}$$

This is effectively a heat equation with the variable x in place of the usual time variable.

4.6 A First Coupled Filter/Channel Model

With the additional assumption that both the filter and channel are thin compared to the length $h/L, H/L \ll 1$ so that the Laplacian (diffusion) terms can be approximated by diffusion in the z direction, we propose the following coupled filter/channel model. In the filter, $0 < x < L$ and $0 < z < h$ we have

$$\frac{\partial \phi_\ell}{\partial t} = \frac{k}{\rho_\ell} C_{\mathrm{SO}_2} \left(1 - \alpha C_{\mathrm{SO}_2}\right) A(\phi_\ell), \tag{64}$$

$$0 = -D_g \frac{\partial}{\partial z} \left(D_{eff}(\phi_\ell) \frac{\partial C_{\mathrm{SO}_2}}{\partial z} \right) + k C_{\mathrm{SO}_2} \left(1 - \alpha C_{\mathrm{SO}_2}\right) A(\phi_\ell). \tag{65}$$

In the channel, $0 < x < L$ and $-H < z < 0$ we have

$$u_c \frac{\partial C_{\mathrm{SO}_2}}{\partial x} = \frac{D_g}{M_{\mathrm{SO}_2}} \frac{\partial^2 C_{\mathrm{SO}_2}}{\partial z^2}. \tag{66}$$

These equations are subject to boundary conditions at the filter/channel boundary

$$C_{\mathrm{SO}_2}(z = 0^-) = C_{\mathrm{SO}_2}(z = 0^+), \tag{67}$$

$$\left. \frac{\partial C_{\mathrm{SO}_2}}{\partial z} \right|_{z=0^-} = D_{eff}(\phi_\ell) \left. \frac{\partial C_{\mathrm{SO}_2}}{\partial z} \right|_{z=0^+}, \tag{68}$$

boundary conditions at the channel inlet

$$C_{\mathrm{SO}_2}(x = 0) = C^{in}_{\mathrm{SO}_2} \qquad \text{for } -H < z < 0, \tag{69}$$

and initial conditions

$$\phi_\ell(t = 0) = 0 \qquad \text{for } 0 < x < L \text{ and } 0 < z < h. \tag{70}$$

A dimensionless set of governing equations can be obtained as follows. Let

$$\bar{x} = \frac{x}{L}, \quad \bar{z} = \frac{z}{h}, \quad \bar{t} = \frac{t}{\rho_\ell / (k A_0 C^{in}_{\mathrm{SO}_2})}, \quad \bar{C} = \frac{C_{\mathrm{SO}_2}}{C^{in}_{\mathrm{SO}_2}}, \quad \bar{A}(\phi_\ell) = \frac{A(\phi_\ell)}{A_0}, \quad \bar{H} = \frac{H}{h}, \tag{71}$$

where A_0 is a reference value for available catalyst surface area. It follows that the dimensionless governing equations, boundary conditions are initial conditions are (dropping bars) given below. In the filter $0 < x < 1$ and $0 < z < 1$

$$\frac{\partial \phi_\ell}{\partial t} = C \left(1 - \alpha C\right) A(\phi_\ell), \tag{72}$$

$$0 = -R \frac{\partial}{\partial z} \left(D_{eff}(\phi_\ell) \frac{\partial C}{\partial z} \right) + C \left(1 - \alpha C\right) A(\phi_\ell). \tag{73}$$

where $R = D_g/(kA_0h^2)$. In the channel, $0 < x < 1$ and $-H < z < 0$ we have

$$U\frac{\partial C}{\partial x} = R\frac{\partial^2 C}{\partial z^2}, \tag{74}$$

where $U = u_c M_{\mathrm{SO}_2}/(kA_0L)$. These equations are subject to boundary conditions at the filter/channel boundary

$$C(z = 0^-) = C(z = 0^+), \tag{75}$$

$$\left.\frac{\partial C}{\partial z}\right|_{z=0^-} = D_{eff}(\phi_\ell)\left.\frac{\partial C}{\partial z}\right|_{z=0^+}, \tag{76}$$

where $D_{eff}(\phi_\ell) = (1 - \phi_s) - D\phi_\ell$ and $D \equiv 1 - D_\ell/D_g$ (with ϕ_s a prescribed constant representing the solid volume fraction in the filter), boundary conditions at the channel inlet

$$C(x = 0) = 1 \qquad \text{for } -H < z < 0, \tag{77}$$

and initial conditions for the liquid volume fraction in the filter

$$\phi_\ell(t = 0) = 0 \qquad \text{for } 0 < x < 1 \text{ and } 0 < z < 1. \tag{78}$$

As stated, the model applies to a situation in which the sulfur dioxide concentration in the filter and channel are quasi-steady (dominated by diffusion in the vertical – cross stream – direction and reaction) and adjust rapidly on the time scale in which water builds up in the filter. The model will allow one to make a prediction about the value of the sulfur dioxide concentration at the channel exit, $C(x = 1, z, t)$ for $-H < z < 0$ as well as the volume of water and its distribution found in the filter $\phi_\ell(x, z, t)$ as a function of time. The parameter α will measure the effect of reaction inhibition based on sulfur dioxide occupying and deactivating catalyst sites. Using a non-constant function $A(\phi_\ell)$ will allow one to investigate the role of fluid build up and its assumed distribution on the catalyst on the filter effectiveness. Further, the diffusion of sulfur dioxide will be slowed directly through the dependence of the diffusion coefficient $D_{eff}(\phi_\ell)$ on the liquid volume fraction.

4.7 Preliminary Numerical Results of the Continuum Filter/Channel Model

The model was solved using a finite difference scheme that, starting at $t = 0$ with no fluid in the filter and given the inlet concentration at $z = 0$, computes the filter boundary value problem first at $x = 0$, then passes information on the solute flux at the filter/channel boundary to the channel PDE solver which advances the concentration in the channel to the next grid point in the horizontal direction. The SO_2 concentration in the channel evaluated at the filter/channel boundary $z = 0$ at the new x position is then used to compute the filter concentration from the filter BVP at the new x position. This process is repeated until the filter and channel concentrations are known throughout the full 2D spatial domain. At this stage, the liquid volume fraction is updated everywhere in the filter via the liquid volume fraction ODE. The procedure to update the concentrations in the filter and channel are then repeated with this new liquid volume fraction distribution.

For simplicity in the numerical solution of this problem and the preliminary results shown below we have implemented the above model with $A(\phi_\ell) = 1 - \beta\phi_\ell$ as a simple model that allows for the reduction of catalyst surface area with the build up of fluid, measured by ϕ_ℓ, in the filter. This model, together with the effective diffusion coefficient $D_{eff}(\phi_\ell) = 1 - \phi_s - D\phi_\ell$ and the factor $(1 - \alpha C)$ in the reaction term allows us to independently assess the three important effects of (1) reduction in catalyst surface area by build up of fluid in the filter, (2) the reduction in diffusion pathways due to the reduction of gas volume fraction and increase in liquid volume fraction and (3) the reduction of reaction rate due to the direct binding by SO_2 to deactivate catalyst sites.

Figures (6)–(8) show some representative output from the above described algorithm (code written in MATLAB). Parameters were chosen for illustrative purposes only and were not intended to specifically match any particular known values or specific filter designs. Detailed descriptions of each figure are given in the captions. A key message is that the coupled filter/channel model presented here is able to make predictions about the efficiency of the filter and to make some assessments about the influence of water generation on the filter efficiency. In particular, Figure (8) shows the ratio of the integrated concentration at the channel exit and the integrated concentration at the channel inlet. That is, we compute the quantity

$$\frac{1}{H}\int_{-H}^{0} C(x = 1, z, t)dz. \tag{79}$$

Note that the inlet concentration of SO_2 is unity everywhere so the integrated inlet concentration is simply H. Figure (8) shows that, as expected, the reduction of catalyst sites directly by SO_2 (measured by parameter α), or by liquid covering catalyst surface area (measured by parameter β) or by a reduction in the diffusion rate by a lower diffusion coefficient in the liquid phase in the filter, all make the filter less efficient. The latter two effects that relate directly to water generation lead to a decrease in filter efficiency over time.

5 Conclusions

We have developed mathematical and computational models aimed to improve the understanding of filters that function by removal of pollutants such as SO_2 by chemical reaction. A limiting feature of these filters is the build-up of sulfuric acid (H_2SO_4), a product of the reaction, inside the filter. We have presented work on three main fronts. First, a detailed description of the central chemical reactions was presented. Second, a computational model was developed for chemical transport and fluid generation in the filter based on a network description of the filter and associated pore space. Third, a continuum model was developed that couples these diffusive and reactive processes in the filter to the flow and depletion of chemical concentration in the channel between filters. Preliminary calculations have been given to demonstrate proof of concept of these models. Further computational investigations of these models could be performed to address questions about more specific filter geometries and characteristics.

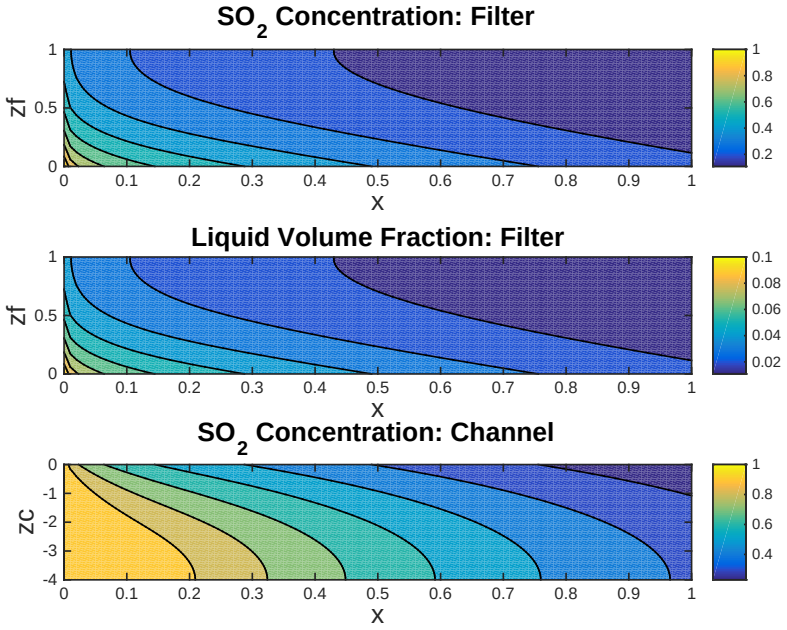

Figure 6: This figure shows SO_2 concentrations in the filter (upper plot) and in the channel (lower plot) and the liquid volume fraction in the filter (middle plot) at an arbitrary final time of $t = 0.1$. This situation corresponds to one in which the generation of water has no influence on the concentration field in either the filter or in the channel: $\alpha = 0$ (no reduction in catalyst sites due to SO_2 occupying sites), $\beta = 0$ (no reduction in available catalyst surface area due to fluid build-up in pore space) and $D = 0$ (no reduction in diffusion due to water build-up – SO_2 diffuses equally fast through both gas and liquid phases). This case is presented as a reference case. The other parameters used in this particular simulation are $R = 1$, $U = 0.05$, $\phi_s = 0.5$, $H = 4$. Numerical discretization in the z direction used 51 evenly-spaced grid points in the filter and 51 evenly spaced points in the channel. The number of time steps, starting from $t = 0$ was 50.

References

[1] R. B. Bird, W. E. Steward and E. N. Lightfoot, *Transport Phenomena*, Second Edition (Wiley, 2007).

[2] M. Cieplak and M. O. Robbins, Influence of contact angle on quasi-static fluid invasion of porous media. *Phys. Rev. B* **41** 11508–11521 (1990)

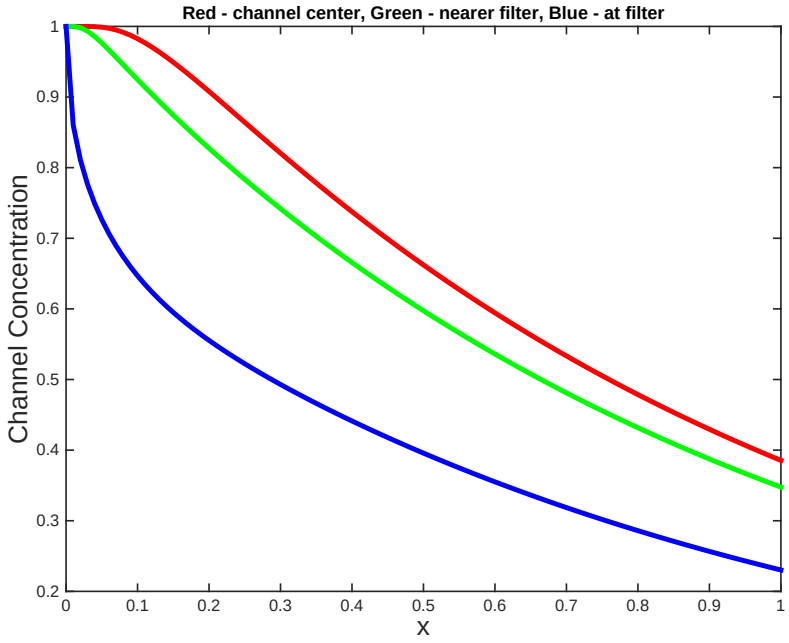

Figure 7: This figure shows SO_2 concentration profiles in the channel as a function of x at the centerline between filters (red curve, $z = -4$), halfway between the channel centerline and the channel/filter boundary (green curve, $z = -2$) and at the channel/filter boundary (blue curve, $z = 0$) at an arbitrary final time of $t = 0.1$. This plot shows that the SO_2 concentration is reduced in the direction of flow (left to right) and that the largest reduction in SO_2 concentration occurs at the channel/filter boundary. Parameters are the same as in the previous figure.

[3] M. El Hannach, J. Pauchet and M. Prat, Pore network modeling: Application to multiphase transport inside the cathode catalyst layer of proton exchange membrane fuel cell. *Electrochimica Acta* **56** 10796–10808 (2011).

[4] M. El Hannach, M. Prat and J. Pauchet, Pore network model of the cathode catalyst layer of proton exchange membrane fuel cells: Analysis of water management and electrical performance. *Int. J. Hydrogen Energy* **37** 18996–19006 (2012).

[5] V. M. H. Govindarao and K. V. Gopalakrishna, Oxidation of sulfur dioxide in aqueous suspensions of activated carbon. *Ind. Eng. Chem. Res.* **34** 2258–2271 (1995).

[6] P.K. Sinha and C.-Y. Wang, Pore-network modeling of liquid water transport in gas diffusion layer of a polymer electrolyte fuel cell. *Electrochimica Acta* **52** 7936–7945 (2007).

[7] M. G. Worster, The dynamics of mushy layers. In *Interactive Dynamics of Convection and Solidification* (ed. S. H. Davis, H. E. Huppert, U. Muller & M. G. Worster), pp. 113–138. Kluwer (1992).

[8] M. G. Worster, Convection in mushy layers. *Annu. Rev. Fluid Mech.* **29**, 91–122 (1997).

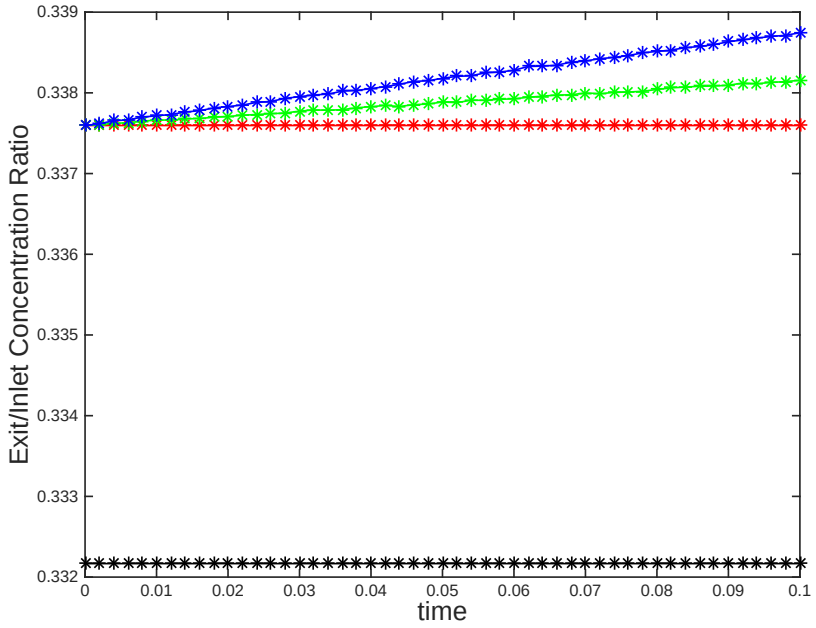

Figure 8: This figure shows the integrated SO_2 concentration at the channel exit relative to the integrated SO_2 concentration at the channel inlet as computed from equation (79). A value of 0 would indicate that the SO_2 was completely removed by the filter while a value of 1 would indicate that no SO_2 was removed by the filter. The black curve shows the case $\alpha = \beta = D = 0$ corresponding to no influence of water generation or catalyst site reduction on the concentration of SO_2. In this case there is no change in filter efficiency with respect to time as the time variation of liquid in the filter, by choice of parameters, does not influence the SO_2 concentration. The red curve shows the case $\alpha = 0.1$, $\beta = D = 0$ corresponding to no influence of water generation but catalyst site reduction due to the presence of SO_2. Relative to the black curve, the filter in this case is less efficient. The green curve shows the case $\alpha = 0.1$, $\beta = 0.1$, $D = 0$ which extends the previous case to include the effect of catalyst surface area reduction due to water generation in the filter. Here we see an increase over time in the SO_2 concentration at the channel exit. Finally, the blue curve shows the case $\alpha = 0.1$, $\beta = 0.1$ and $D = 0.1$ indicating the influence of a reduction in the effective diffusion coefficient in the filter associated with a smaller diffusion coefficient in the liquid phase compared to the gas phase. Parameters are the same as in the previous figure and were intended to show general trends associated with these various effects rather than to capture quantitative predictions on the filter efficiency for a realistic filter.